VNU Journal of Science: Natural Sciences and Technology

Journal homepage: https://js.vnu.edu.vn/NST

Original Article

Efficient Photoreduction of CO_2 to CH_4 on AgCl/Ag/g-C_3N_4 Ternary Composites

Dinh Thi Thuy Hang[1,2], Nguyen Dinh Bang[1], Nguyen Thanh Binh[1,*]

[1]*VNU University of Science, 19 Le Thanh Tong, Cua Nam, Hanoi, Vietnam*
[2]*Vietnam Maritime University, 484 Lach Tray, Le Chan, Hai Phong, Vietnam*

Received 13th May 2025
Revised 28th January 2026; Accepted 06th Ferbuary 2026

Abstract: The AgCl/Ag/g-C_3N_4 ternary composites were synthesized by simple methods. The characterizations (XRD, FTIR, TEM, UV-DRS, PL) indicated clearly the existence of Ag, AgCl, and g-C_3N_4 phases and visible light absorption ability of composites. The photocatalytic activity was evaluated by photoreducing CO_2 to CH_4. The obtained results showed that the composite 3AC-Ag-CN exhibited the highest activity with CH_4 production of $3.38.10^{-2}$ $\mu mol.g^{-1}.h^{-1}$, which was ~7.5 times higher than that of g-C_3N_4. This activity enhancement was explained by their Z-scheme heterojunction structure.

Keywords: Graphitic carbon nitride, photoreduction, silver.

1. Introduction

Climate change, driven by global warming, is a major challenge for global sustainable development. Among the gases that cause the greenhouse effect, CO_2 contributes the most. CO_2 is emitted mainly from the process of using fossil fuels such as coal and petroleum. Along with the rapid development of the global economy, CO_2 emissions are increasing at an alarming rate. To reduce CO_2 emissions, photocatalytic reduction of CO_2 into fuels such as CH_4, CH_3OH, and C2H5OH proves to be a promising pathway [1]. Among these compounds, CH_4 also causes the greenhouse effect. However, its lifetime is only about a decade instead of centuries like CO_2 [2]. Therefore, CO_2 converting to CH_4 is a suitable solution for greenhouse gas recycling during the transition from fossil fuels to green energy.

The most basic photocatalyst is TiO_2 oxide, but as a relatively large band gap energy, E_g = 3.2 eV, this catalyst is activated only under UV light irradiation. Recently, the semiconductor material, organic polymer, and carbon graphitic nitride g-C_3N_4 have attracted the attention of researchers [3]. This material is interesting because of its easy synthesis method, low-cost raw materials (such as urea and melamine), and, especially, its relatively low band gap energy, $E_g \approx$ = 2.7 eV. With the $E_g \approx$ 2.7 eV, g-C_3N_4 can be activated by visible

* Corresponding author.
E-mail address: nguyenthanhbinh@hus.edu.vn

https://doi.org/10.25073/2588-1140/vnunst.5661

light. Thus, it is possible to utilize sunlight as a source of activation energy, which is inexhaustible and free. However, the g-C_3N_4 material has a drawback, which is the rapid recombination of photogenerated electron-hole pairs, leading to decreased activity [3, 4]. Therefore, scientists have recently developed composite materials that combine g-C_3N_4 with salts [5-7], metals [8-10], and oxides [11-14] to inhibit this phenomenon.

Recently, several scientists paid attention to ternary composites, which consist of three types of components above [15-17]. That could combine the advantages of each component, making the composite more active. Therefore, in this study, we synthesized Ag/AgCl/g-C_3N_4 composite and evaluated its photocatalytic activity through CO_2 photoreduction.

2. Experimental

2.1. Catalyst Preparation and Characterization

Graphitic carbon nitride (g-C_3N_4) was synthesized by simple calcination of melamine (Sigma-Aldrich) at 550°C for 3 hours under N_2 flow. Series x% (wt)Ag/AgCl/g-C_3N_4 composites (x%: percentage of silver metal, including Ag amount in AgCl) were prepared as follows:

Firstly, 2 g of g-C_3N_4 and 50 mL of ethylene glycol (EG) were placed in a three-necked flask and covered with paraffin paper. The mixture was then sonicated for 20 minutes. After that, a calculated volume of $AgNO_3$-EG 0,025M solution was added to the mixture, which was stirred for 30 minutes to obtain a yellow-brown mixture. Then, 10 ml of NaOH-EG 0,25 M was added, and the mixture was stirred and heated to 160 °C for 2 hours. After cooling to room temperature, 10 mL HCl-EG 0.25M was added, and the mixture was stirred for 90 minutes. Finally, the obtained mixture was washed and centrifuged twice with deionized water, then dried in an oven to obtain AgNP/g-C_3N_4.

All composites were characterized by X-ray difraction (XRD, model Bruker D8), Fourier Transform InfraRed (FTIR, model 8101M Shimazu), and UV-vis diffuse reflectance spectroscopy (UV-DRS, model Jaco V-530), Photoluminescence spectroscopy (PL, model Horiba FluoroMax-4) and Transmission Electron Microscopy (TEM, JEOLJEM-1010).

2.2. Photocatalysis Procedure

The photocatalytic activity of the composite was evaluated through CO_2 photoreduction. The procedure was carried out as follows:

In a 5 cm-diameter beaker, 100 mg of the composite and 15 ml HPLC water were added. This mixture was dried in the oven at 70^{o}C in order to well disperse the composite onto the bottom of the beaker. Then, the catalyst-containing beaker was placed in a closed, handmade reactor with a quartz window. The high-purity CO_2 (99.99%) flow of 500 ml/min bubbled through a 200 ml HPLC water container, which remained at 25 ^{o}C before purging the reactor for 15 min. After that, the reactor was closed via the valve system, and the 150W Xenon lamp (Newport model 67005) was turned on to irradiate the composite in the reactor for 18 hours. Finally, the gas composition in the reactor was analyzed by Gas Chromatography (Scion 456) equipped with TCD and FID through a system of gas valves.

3. Results and Discussion

3.1. Catalyst Characterization

Figure 1 presents the obtained XRD patterns.

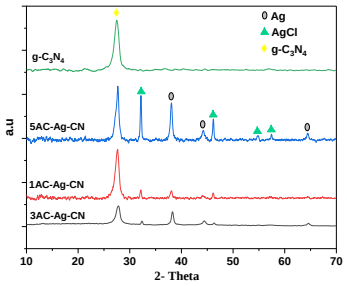

Figure 1. XRD patterns of xAC-Ag-CN composites.

From Figure 1, it can be seen that g-C_3N_4 material has been successfully synthesized with a main characteristic peak appearing at 2θ = 27.3° (JCPDS 87-1526). In the composites' XRD patterns, the peak at 27.5° is always observed, which proves that the composites' synthesis process still retained the g-C_3N_4 structure. Besides, the Ag metal was recognized by characteristic peaks at 38.2°, 44.3°, and 64.4°. The characteristic peaks at 32.3°, 46.2°, 54.8°, and 57.4° are assigned to the face-centred cubic AgCl phase (JCPDS 31-1238). Thus, XRD patterns showed the existence of all 3 phases in the obtained composites: Ag, AgCl, and g-C_3N_4.

To clarify more structural properties of g-C_3N_4 and synthesized composites, the FTIR measurements were carried out and are shown in Figure 2.

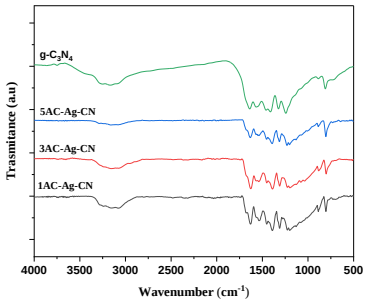

Figure 2. FTIR Spectra of xAC-Ag-CN composites.

As shown in Figure 2, the g-C_3N_4 spectra exhibit a peak at 802 cm^{-1}, which is ascribed to the bending mode of the s-triazine [16]. The peaks in the range 1200-1600 cm^{-1} correspond to stretching vibration of C-N and C=N bonds of the heterocyclic amines present in the g-C_3N_4 structure [18, 19]. The broad band from 3000 to 3500cm^{-1} was attributed to the stretching vibration of the hydroxyl functional group of absorbed water [18, 19]. For the xAC-Ag-CN composites spectra, it was observed that they were similar to those of g-C_3N_4. This similarity proved that the g-C_3N_4 structure was not modified during the composite synthesis. This result is also in accordance with the XRD patterns observed above.

Figure 3 exhibited the TEM images of 3AC-Ag-CN. The black spheres were Ag nanoparticles with an average diameter of 20 nm. It seems that these nanoparticles were not well dispersed. The fuzzy gray area must be the g-C_3N_4 layer and/or AgCl crystals. The contrast between AgCl crystals and g-C_3N_4 layers was not sufficient to observe them.

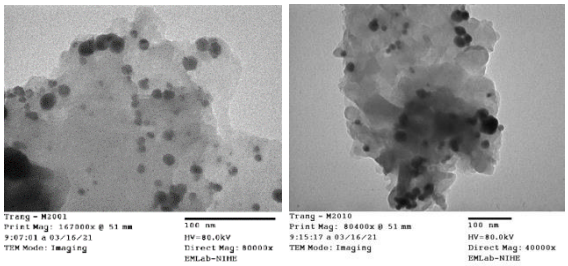

Figure 3. The TEM images of 3AC-Ag-CN composite.

To estimate the composite's light-absorption ability, all composites were characterized using UV-DRS. Figure 4a shows the obtained spectra. Based on these spectra, the plot of the Kubelka-Munk function is presented in Figure 4b. That indicated that the band gap energies are 2.63 eV for g-C_3N_4 and about 2,67 eV for xAC-Ag-CN composites. Hence, all composites could be activated by visible light irradiation.

To obtain a preliminary estimate of the photogenerated electron-hole pair recombination, the PL spectra of g-C_3N_4 and 3AC-Ag-CN were measured and are shown in Figure 5. The spectra showed that the intensity of g-C_3N_4 was ~16 times higher than that of 3AC-Ag-CN. This indicated strong prevention of photogenerated electron-hole pair recombination on 3AC-Ag-CN.

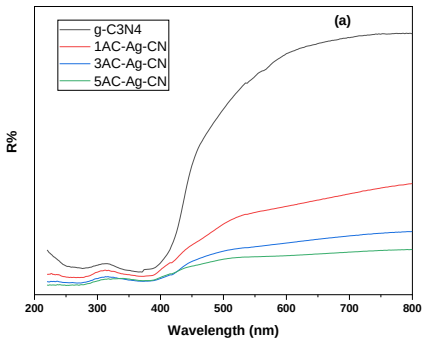

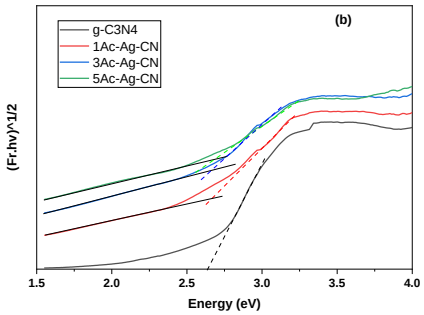

Figure 4. UV-DRS spectra of g-C_3N_4 and xAC-Ag-CN composites.

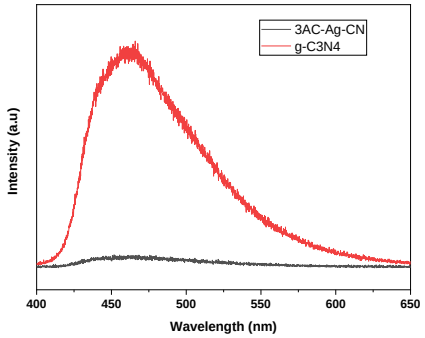

Figure 5. PL spectra of g-C_3N_4 and 3AC-Ag-CN composite.

3.2. Evaluation of Photocatalytic Activity

The photocatalytic activity of the composite was evaluated through CO_2 photoreduction.

In these experiments, CH_4 was the unique detected product. Figure 6 presents the CO_2 amount obtained over g-C_3N_4 and composites.

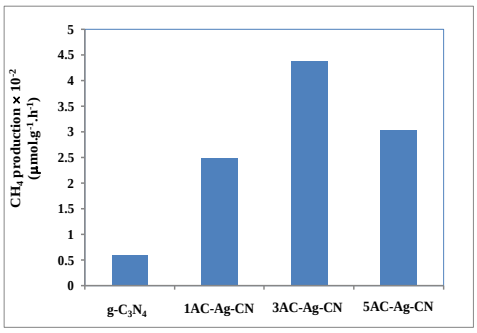

Figure 6. CH_4 production on g-C_3N_4 and xAC-Ag-CN composites.

The results showed that 3AC-Ag-CN exhibited the highest activity with CH_4 production of $3.38.10^{-2}$ μmol.g^{-1}.h^{-1}, followed by 5AC-Ag-CN ($2.33.10^{-2}$ μmol.g^{-1}.h^{-1}), 1AC-Ag-CN ($1.92.10^{-2}$ μmol.g^{-1}.h^{-1}) and g-C_3N_4 ($0.45.10^{-2}$ μmol.g^{-1}.h^{-1}). Thus, CH_4 amount on 3AC-Ag-CN was ~7.5 times higher than that of g-C_3N_4.

To better understand this photocatalytic improvement, a CO_2 photoreduction mechanism was proposed in Figure 7.

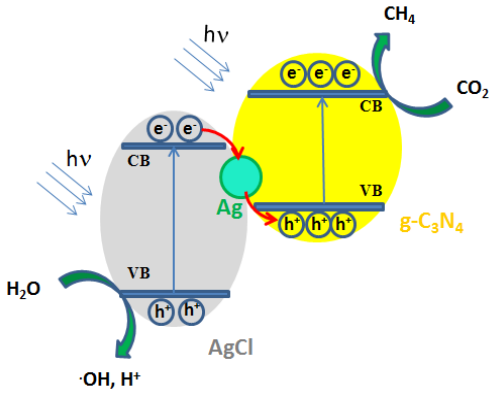

Figure 7. Schematic diagram of photogenerated charge transfer for AgCl/Ag/g-C_3N_4 composites.

In fact, according to this mechanism, both the AgCl and g-C_3N_4 were activated under xenon lamp irradiation to form photogenerated electron-hole pairs (e^-/h^+) on the conduction band (CB) and valence band (VB). Then, the e^- on AgCl(CB) transferred to g-C_3N_4(VB) through Ag nanoparticles, which plays as "electron-attracted trap" by its excellent conductivity. The CO_2 was reduced into CH_4 on g-C_3N_4(CB) and on the AgCl(VB), H_2O was oxidized to hydroxyl radical ·OH. This type of structure and its operation are called Z-scheme heterojunction [20-22]. The processes are summarized by the equations below:

$AgCl + h\nu \rightarrow e^-(AgCl(CB)) + h^+(AgCl(VB))$

$g\text{-}C_3N_4 + h\nu \rightarrow e^-(g\text{-}C_3N_4(CB)) + h^+(g\text{-}C_3N_4(VB))$

$e^-(AgCl(CB)) \rightarrow h^+(g\text{-}C_3N_4(VB))$ (charge transfer)

$8e^-(g\text{-}C_3N_4(CB)) + CO_2 + 8H^+ \rightarrow CH_4 + 2H_2O$

$8h^+(AgCl(VB)) + 8H_2O \rightarrow 8H^+ + 8{}^{\cdot}OH$

$8{}^{\cdot}OH \rightarrow 4H_2O + 2O_2$

Thus, the composites exhibited greater photoactivity than pristine g-C_3N_4. This is reasonably explained by the Z-scheme photocatalytic mechanism outlined above. According to this mechanism, the charge transfer between AgCl(CB) and g-C_3N_4(VB) prevented the recombination of electron–hole pairs. This characteristic was observed in the PL spectra above. In addition, this recombination prevention enriched also e^- on the g-C_3N_4 (VB) and h^+ on AgCl(CB), where it took place CO_2 photoreduction and H_2O oxidation as mentioned above. It is noted that g-C_3N_4(CB) potential(-1,14 eV) is more negative than that of AgCl(CB)(-0,13 eV) [23]. Likewise, AgCl(VB) potential (+3.02 eV) is more positive than that of g-C_3N_4(VB) (+1.58 eV) [23]. It means that the Z-scheme heterojunction has created a new photocatalyst with stronger redox ability. That increased the photocatalytic activity compared with the single-phase composite. Besides, Ag nanoparticles also played an important role in promoting photogenerated electron transfer, one of the key processes for improving photocatalytic activity. [24-27].

4. Conclusions

In conclusion, the ternary AgCl/Ag/g-C_3N_4 composites were successfully synthesized. The XRD and FTIR spectra confirmed the presence of all three components in the composites. The UV-DRS spectra showed that all composites could be activated in the visible light region. The morphology of the 3AC-Ag-CN composite was displayed by TEM images. That indicated Ag nanoparticles with an average diameter of 20 nm dispersed on the g-C_3N_4 layer. The photocatalytic activity evaluated through CO_2 photoreduction into CH_4 exhibited the best activity of all composites in comparison with pristine g-C_3N_4. Concretely, the 3AC-Ag-CN showed the highest photoactivity with CH_4 production of $3.38.10^{-2}$ $\mu mol.g^{-1}.h^{-1}$, ~7.5 times higher than that of pristine g-C_3N_4. The photoactivity enhancement was explained by the Z-scheme heterojunction in these composites, as indicated by the PL spectra. The initial results for CO_2 photoreduction on these composites are quite promising. It opens up new avenues for developing these ternary composites, such as the size of Ag nanoparticles and its dispersion control, and the improvement of contact between the different components in the composite.

References

[1] A. Hezam, T. Peppel, J. Strunk, Pathways Towards a Systematic Development of Z-scheme Photocatalysts for CO_2 Reduction, *Curr. Opin. Green Sustain. Chem.*, Vol. 41, 2023, pp. 100789, https://doi.org/10.1016/j.cogsc.2023.100789.

[2] Control Methane to Slow Global Warming - Fast, Nature, Vol. 596, 2021, pp. 461, https://doi.org/10.1038/d41586-021-02287-y.

[3] J. Wen, J. Xie, X. Chen, X. Li, A Review on g-C_3N_4-based Photocatalysts, *Appl. Surf. Sci.*, Vol. 391, 2017, pp. 72-123, https://doi.org/10.1016/j.apsusc.2016.07.030.

[4] L. Wang, K. Wang, T. He, Y. Zhao, H. Song, H. Wang, Graphitic Carbon Nitride-Based Photocatalytic Materials: Preparation Strategy and Application, *ACS Sustain. Chem. Eng.*, Vol. 8, No. 43, 2020, pp. 16048-16085, https://doi.org/10.1021/acssuschemeng.0c05246.

[5] P. Murugesan, S. Narayanan, M. Manickam, Experimental Studies on Photocatalytic Reduction of CO_2 Using AgBr Decorated g-C_3N_4 Composite in TEA Mediated System, *J. of CO_2 Ulti.*, Vol. 22, 2017, pp. 250-261, https://doi.org/10.1016/j.jcou.2017.10.012.

[6] P. Murugesan, S. Narayanan, M. Matheswaran, M. Praveen Kumar, S. Ravichandran, A Direct Z-Scheme Plasmonic AgCl@g-C_3N_4 Heterojunction Photocatalyst with Superior Visible Light CO_2 Reduction in Aqueous Medium, *Appl. Surf. Sci.*, Vol. 450, 2018, pp. 516-526, https://doi.org/10.1016/j.apsusc.2018.04.111.

[7] T. Di, B. Zhu, B. Cheng, J. Yu, J. Xu, A Direct Z-Scheme g-C_3N_4/SnS_2 Photocatalyst with Superior Visible-light CO_2 Reduction Performance, *J. of Catal.*, Vol. 352, 2017, pp. 532-541, https://doi.org/10.1016/j.jcat.2017.06.006.

[8] S. Cao, Y. Li, B. Zhu, M. Jaroniec, J. Yu, Facet Effect of Pd Cocatalyst on Photocatalytic CO_2 Reduction over g-C_3N_4, *J. Catal.*, Vol. 349, 2017, pp. 208-217, https://doi.org/10.1016/j.jcat.2017.02.005.

[9] K. Koci, H. Dang Van, M. Edelmannová, M. Reli, J. C.S.Wu, Photocatalytic Reduction of CO_2 Using Pt/C_3N_4 Photocatalysts, *Appl.Surf. Sci*., Vol. 503, 2020, pp. 144426, https://doi.org/10.1016/j.apsusc.2019.144426.

[10] Z. Otgonbayar, K. Y. Cho, W. C. Oh, Novel Micro and Nanostructure of a $AgCuInS_2$–Graphene–TiO_2 Ternary Composite for Photocatalytic CO_2 Reduction for Methanol Fuel, *ASC Omega*, Vol. 5, No. 41, 2020, pp. 26389-26401, https://doi.org/10.1021/acsomega.0c02498.

[11] Y. He, L. Zhang, M. Fan, X. Wang, M. L. Walbridge, Q. Nong, Y. Wu, L. Zhao, Z-scheme SnO_{2-x}/g-C_3N_4 Composite as an Efficient Photocatalyst for Dye Degradation and Photocatalytic CO_2 Reduction, *Sol. Energy Mater. Sol. Cells*, Vol. 137, 2015, pp. 175-184, https://doi.org/10.1016/j.solmat.2015.01.037.

[12] Z. Sun, W. Fang, L. Zhao, H. Chen, X. He, W. Li, P. Tian, Z. Huang, g-C_3N_4 Foam/Cu_2O QDs with Excellent CO_2 Adsorption and Synergistic Catalytic Effect for Photocatalytic CO_2 Reduction, *Environ. Int.*, Vol. 130, 2019, pp. 104898, https://doi.org/10.1016/j.envint.2019.06.008.

[13] H. Wang, H. Li, Z. Chen, J. Li, X. Li, P. Huo, Q. Wang, TiO_2 Modified g-C_3N_4 with Enhanced Photocatalytic CO_2 Reduction Performance, *Solid State Sci.*, Vol. 100, 2020, pp. 106099, https://doi.org/10.1016/j.solidstatesciences.2019.106099.

[14] Q. Guo, L. Fu, T. Yan, W. Tian, D. Ma, J. Li, Y. Jiang, X. Wang, Improved Photocatalytic Activity of Porous ZnO Nanosheets by Thermal Deposition Graphene-like g-C_3N_4 for CO_2 Reduction with H_2O Vapor, *Appl. Surf. Sci.*, Vol. 509, 2020, pp. 144773, https://doi.org/10.1016/j.apsusc.2019.144773.

[15] S. Yin, L. Sun, Y. Zhou, X. Li, J. Li, X. Song, P. Huo, H. Wang, Y. Yan, Enhanced Electron–Hole Separation in SnS_2/Au/g-C_3N_4 Embedded Structure for Efficient CO_2 Photoreduction, *Chem. Eng. J*., Vol. 406, 2021, pp. 126776, https://doi.org/10.1016/j.cej.2020.126776.

[16] X. Zhao, J. Guan, J. Li, X. Li, H. Wang, P. Huo, Y. Yan, CeO_2/3D g-C_3N_4 Heterojunction Deposited with Pt Cocatalyst for Enhanced Photocatalytic CO_2 Reduction, *Appl. Surf. Sci.*, Vol. 537, 2021, pp. 147891, https://doi.org/10.1016/j.apsusc.2020.147891.

[17] C. Prasad, H. Tang, I. Bahadur, Graphitic Carbon Nitride-based Ternary Nanocomposites: From Synthesis to Their Applications in Photocatalysis: A Recent Review, *J. Mol. Liq.*, Vol. 281, 2019, pp. 634-654, https://doi.org/10.1016/j.molliq.2019.02.068.

[18] U. Ghosh, A. Majumdar, A. Pai, Photocatalytic CO_2 Reduction over g-C_3N_4 Based Heterostructures: Recent Progress and Prospects, *J. Environ. Chem. Eng.*, Vol. 9, No. 1, 2021, 104631, https://doi.org/10.1016/j.jece.2020.104631.

[19] Y. Guo, S. Chen, Y. Yu, H. Tian, Y. L. Zhao, J. C. Ren, C. Huang, H. Bian, M. Huang, L. An, Y. Li, R. Zhang, Hydrogen-Location-Sensitive Modulation of the Redox Reactivity for Oxygen-Deficient TiO_2, *J. Am. Chem. Soc.*, Vol. 141, No. 21, 2019, pp. 8407-8411, https://doi.org/10.1021/jacs.9b01836.

[20] M. Jourshabani, B. K. Lee, Z. Shariatinia, From Traditional Strategies to Z-scheme Configuration in Graphitic Carbon Nitride Photocatalysts: Recent Progress and Future Challenges, *Appl. Catal. B: Environ.*, Vol. 276, 2020, pp. 119157, https://doi.org/10.1016/j.apcatb.2020.119157.

[21] G. Liao, C. Li, X. Li, B. Fang, Emerging Polymeric Carbon Nitride Z-scheme Systems for Photocatalysis, *Cell Rep. Phy. Sci.*, Vol. 2, No. 3, 2021, pp. 100355, https://doi.org/10.1016/j.xcrp.2021.100355.

[22] P. Murugesan, S. Narayanan, M. Manickam, P. K. Murugesan, R. Subbiah, A Direct Z-Scheme Plasmonic AgCl@g-C_3N_4 Heterojunction Photocatalyst with Superior Visible Light CO_2 Reduction in Aqueous Medium, *Appl. Surf. Sci.*, Vol. 450, 2018, pp. 516-526, https://doi.org/10.1016/j.apsusc.2018.04.111.

[23] G. Fan, R. Ning, Z. Yan, J. Luo, B. Du, J. Zhan, L. Liu, J. Zhang, Double Photoelectron-transfer Mechanism in Ag–AgCl/WO_3/g-C_3N_4 Photocatalyst with Enhanced Visible-light Photocatalytic Activity for Trimethoprim Degradation, *J. Hazard. Mater*., Vol. 403, 2021, pp. 123964, https://doi.org/10.1016/j.jhazmat.2020.123964.

[24] Y. He, L. Zhang, B. Teng, M. Fan, New Application of Z-Scheme Ag_3PO_4/g-C_3N_4 Composite in Converting CO_2 to Fuel, *Environ. Sci. Technol*, Vol. 49, No. 1, 2015, pp. 649-656, https://doi.org/10.1021/es5046309.

[25] G. Zhang, X. Zhu, D. Chen, N. Li, Q. Xu, H. Li, J. He, H. Xu, J. Lu, Hierarchical *Z*-Scheme g-C_3N_4/Au/$ZnIn_2S_4$ Photocatalyst for Highly Enhanced Visible-light Photocatalytic Nitric Oxide Removal and Carbon Dioxide Conversion, *Environ. Sci.: Nano*, Vol. 7, No. 2, 2020, pp. 676-687, https://doi.org/10.1039/C9EN01325C.

[26] W. Liu, J. Shen, X. Yang, Q. Liu, H. Tang, Dual Z-Scheme g-C_3N_4/Ag_3PO_4/Ag_2MoO_4 Ternary Composite Photocatalyst for Solar Oxygen Evolution from Water Splitting, *Appl. Surf. Sci.*, Vol. 456, 2018, pp. 369-378, https://doi.org/10.1016/j.apsusc.2018.06.156.

[27] K. Wang, J. Li, G. Zhang, Ag-Bridged Z-Scheme 2D/2D $Bi_5FeTi_3O_{15}$/g-C_3N_4 Heterojunction for Enhanced Photocatalysis: Mediator-Induced Interfacial Charge Transfer and Mechanism Insights, *ACS Appl. Mater. Interfaces*, Vol. 11, No. 31, 2019, pp. 27686-27696, https://doi.org/10.1021/acsami.9b05074.